Transport and losses of fusion-born alpha particles in the presence of tearing modes using the new Toroidal Accelerated Particle Simulator (TAPaS)

David Zarzoso, Diego Del-Castillo-Negrete, Rémi Lacroix, Pierre-Eric Bernard, Stanislas Touzet

Transport and losses of fusion-born alpha particles in the presence of tearing modes using the new Toroidal Accelerated PArticle Simulator (TAPaS)

David Zarzoso[1], Diego del-Castillo-Negrete[2], Rémi Lacroix[3], Pierre-Eric Bernard[4] and Stanislas Touzet[3]

[1] Aix-Marseille Université, CNRS, PIIM, UMR 7345 Marseille, France
[2] Oak Ridge National Laboratory, Oak Ridge, TN 37831-8071, United States of America
[3] Institut du développement et des ressources en informatique scientifique (IDRIS), CNRS, Université Paris-Saclay, F-91403, Orsay, France
[4] Hewlett Packard Enterprise (HPE), France.

E-mail: david.zarzoso-fernandez@univ-amu.fr

Abstract. The transport and losses of fusion-born alpha particles is studied in the presence of a single-helicity tearing mode, characterized by $(m = 2, n = 1)$. The analysis is performed by means of the recently developed Toroidal Accelerated PArticle Simulator (TAPaS). Although such modes have been usually believed to result only in a local flattening of the radial profiles, it is shown that the density profile can exhibit a global modification leading to significant losses of alpha particles. This is due to the fact that, although the magnetic field does not exhibit any chaotic behaviour, the trajectories of alpha particles do, as revealed by their Poincaré maps. Such result is in qualitative agreement with past observations and simulations of energetic particles generated by neutral beam injection in TFTR, DIII-D and AUG tokamaks. In-depth analysis is carried out to characterize the impact of the tearing mode on the transport and losses of fusion-born alpha-particles with a realistic density profile. The impact of the amplitude is evidenced. Moreover, the effect of the island rotation frequency is assessed based on a detailed analysis of the linear resonances in phase-space, in agreement with the simulation results. Finally, the probability density function of the exit time has been computed and the transport of alpha particles has been found to be anomalous.

1. Introduction

In future fusion devices such as ITER, a significant population of alpha particles is expected to be produced by the nuclear fusion reactions between Deuterium and Tritium. Such fusion-born alpha particles exhibit velocities which are much larger than the thermal velocity of the bulk plasma. This is the reason why they are also called *energetic particles* (EP) and they must be sufficiently well confined to transfer their energy to the bulk plasma through Coulomb collisions or to ensure the current drive

efficiency [1, 2]. In addition, a fusion plasma is a complex nonlinear system, characterized by strong gradients which lead to instabilities developing on disparate spatio-temporal scales, ranging from the electron Larmor radius to the size of the tokamak ($\sim$ 1 meter) and from the microsecond to the confinement time ($\sim$ 1 second). Such instabilities can have a deleterious effect on the confinement of EP, limiting therefore the performance of fusion devices. Already in the electrostatic regime, the effect of single helicity electrostatic perturbations on EP transport and losses was analysed in detailed in Refs. [3, 4]. In the present work we focus on single helicity rotating and non-rotating magnetic perturbations representing a tearing mode [5, 6, 7] and analyse their impact on the transport and losses of fusion-born alpha particles. Due to the curvature of the magnetic field lines, the trajectories of EP exhibit a departure from the magnetic flux surfaces, which is called magnetic drift. This departure is more pronounced when the energy of particles is high. Since alpha particles are born with 3.5 MeV, taking into account their magnetic drift is of prime importance. The magnetic drift introduces an additional periodicity in the trajectories of particles in a tokamak, which can couple to the periodicity of electro-magnetic perturbations, resulting therefore in higher order harmonics. Such phenomenon was first raised by Mynick [8] for EP generated by external heating in tokamaks and observed by Zweben [9] for alpha particles in TFTR. It was also confirmed by Carolipio in DIII-D tokamak [10] and invoked by Garcia-Muñoz to explain the losses of NBI-generated EP in the presence of tearing modes in AUG tokamak [11]. Further analysis regarding the interaction of EP and tearing modes in phase space was presented in Ref. [12]. To our knowledge, the most recent studies of EP losses induced by tearing modes have been reported in Ref. [13] in the framework of simulations of passing energetic ions in EAST tokamak.

A tearing mode can be excited in tokamaks due to the gradient of the plasma current in the presence of non-ideal effects and can tear apart the magnetic field lines, resulting in their reconnection [14]. This process leads to a modification of the magnetic topology, characterized by the formation of magnetic islands. In magnetically confined plasmas, tearing modes enhance particle and energy transport, degrading this way the overall confinement [15]. In the present paper, we explore the mechanism highlighted in the seminal work of Mynick [8] and extend it to the transport and losses of alpha particles in JET-like tokamaks in view of the next JET experimental campaign. For this purpose, we use a recently developed Toroidal Accelerated PArticle Simulator (TAPAS). In the same spirit, other codes such as ORBIT [16], OMFC [17], LOCUST [18], SPIRAL [19] or ASCOT [20] were developed in the past with the purpose of studying the transport of energetic particles in tokamaks. Also the analysis of other high-energy particles such as runaway electrons has been possible using KORC [21], which includes relativistic corrections to the full-orbit equations. Moreover, reduced models such as the kick model reported in [22] can be used to take into account the basic mechanism of wave-particle interaction. Such model was recently applied to the study of EP transport induced by neoclassical tearing modes in DIII-D [23] and by the coupled kink and tearing modes in NSTX [24] and is based on the reconstruction of a probability density function for the

particle steps in phase space, which might exhibit uncertainties due to poor statistics in some regions of phase space. TAPAS has been optimized, parallelized and accelerated using graphical processing units (GPU), which results in a very high performance. To our knowledge, only LOCUST has been accelerated on GPU as reported in a very recent publication [25]. Such acceleration allows TAPAS to accurately and efficiently perform the long-time integration of the trajectories of very large ensembles of particles ($> 10^7$) and to carry out dedicated diagnostics to tackle computational intense statistical particle studies for which most existing codes might not be suitable. Some specific examples include the study of statistical rare events that underline non-diffusive transport in the presence of gyrokinetic turbulence and/or MHD activity. This increased statistics in space and time is essential to characterize and quantify the transport of EP, such as alpha particles, in tokamak plasmas, which is the purpose of the present work. Also of interest is the dependence of transport on different orbit models, e.g. full-orbit, gyro-averaged, or guiding center. These studies also benefit from TAPAS' flexible particle initialization routines. In addition, TAPAS design, and in particular the orbit model presented here, has been developed for the seamless coupling with GYSELA5D [26] which is a problem we are currently working on. At the same time the decoupling of the integrator and orbit model modules allow the seamless incorporation of different integration algorithms and orbit models incorporating different levels of approximations and spatio-temporal scales.

The remainder of the paper is structured as follows. Section 2 is devoted to the description of TAPAS. In section 3 we provide the details of the simulations together with the magnetic perturbation used to model the tearing mode. Analysis of the effect of the island width and rotation frequency is done in section 4. We report in section 5 the results characterizing the transport and losses of fusion-born alpha particles. Finally, the conclusions and future direction are presented in section 6.

2. The Toroidal Accelerated PArticle Simulator (TAPAS)

2.1. The model

TAPAS allows the integration of a large amount of particle trajectories taking advantage of the GPU parallelization. In the present work, we use TAPAS to solve the time evolution of the guiding-centre coordinates $\left(x, u_\parallel, \mu\right)$ of N_{part} particles in a prescribed 3D electro-magnetic perturbation $\left(\phi, A_\parallel\right)$ and an equilibrium magnetic field $\mathbf{B}_{\text{eq}}$. Particles are characterized by their mass m and their charge eZ. The equilibrium magnetic field can be arbitrary (obtained from a numerical equilibrium) or imposed analytically. The code integrates the equations of motion, for each particle, in co-variant formulation (in the absence of collisions in the present paper)

$$\frac{\mathrm{d}x^i}{\mathrm{d}t} = u_\parallel b^i + v_D^i + v_H^i + v_{\delta A}^i \tag{1}$$

$$m\frac{\mathrm{d}u_\parallel}{\mathrm{d}t} = -\left(b^i + \frac{mu_\parallel}{eZB^*_\parallel}\tau^i\right)\partial_i\left[\mu B_{\mathrm{eq}} + h\right] \tag{2}$$

$$\frac{\mathrm{d}\mu}{\mathrm{d}t} = 0 \tag{3}$$

where $(x^1, x^2, x^3) \equiv (r, \theta, \varphi)$ and the sum over repeated indices is implicit. Here, θ and φ are the poloidal and toroidal coordinates, respectively, and r is a flux surface label, having length dimensions. When the magnetic equilibrium has circular cross-section, r represents the radial position, hence the chosen notation. The perturbed particle Hamiltonian h is expressed as

$$h = J_0\left(\phi\right) - u_\parallel J_0\left(A_\parallel\right) \tag{4}$$

where $J_0\left(\cdot\right)$ is the gyro-average operator. The parallel Hamiltonian velocity $u_\parallel$ is written in terms of the parallel velocity $v_\parallel$ of the guiding centre

$$u_\parallel = v_\parallel + \frac{eZ}{m}A_\parallel \tag{5}$$

The drift velocities are given by the following expressions

$$\mathbf{v}_D = \frac{\mu B_{\mathrm{eq}}}{eZB^*_\parallel}\mathbf{b}\times\frac{\nabla B_{\mathrm{eq}}}{B_{\mathrm{eq}}} + \frac{mu^2_\parallel}{eZB^*_\parallel}\boldsymbol{\tau} \tag{6}$$

$$\mathbf{v}_H = \frac{\mathbf{b}}{B^*_\parallel}\times\left(\nabla J_0\left(\phi\right) - u_\parallel\nabla J_0\left(A_\parallel\right)\right) \tag{7}$$

$$\mathbf{v}_{\delta A} = -\frac{eZ}{m}J_0\left(A_\parallel\right)\left(\mathbf{b} + \frac{mu_\parallel}{eZB^*_\parallel}\boldsymbol{\tau}\right) \tag{8}$$

Representing, respectively, the magnetic drift velocity, the Hamiltonian drift velocity and the magnetic drift velocity modified by the parallel flow due to the magnetic potential. Note that the Hamiltonian drift velocity is the sum of the $E\times B$ drift velocity and a perpendicular velocity due to the magnetic field line bending. The vector $\mathbf{b}$ is defined as $\mathbf{b} = \mathbf{B}_{\mathrm{eq}}/B_{\mathrm{eq}}$, with $B_{\mathrm{eq}} = \|\mathbf{B}_{\mathrm{eq}}\|$ and the vector $\boldsymbol{\tau}$ is given by

$$\boldsymbol{\tau} = \mathbf{b}\times\left(\mathbf{b}\cdot\nabla\mathbf{b}\right) \tag{9}$$

In the previous expressions, $B^*_\parallel$ is written as

$$B^*_\parallel = B_{\mathrm{eq}} + \frac{mu_\parallel}{eZ}\mathbf{b}\cdot\left(\nabla\times\mathbf{b}\right) \tag{10}$$

and is related to the Jacobian of the guiding-centre transformation

$$J_v = \frac{2\pi B^*_\parallel}{m} \tag{11}$$

Finally, the co-variant component of a vector Y is given by $Y^i = Y\cdot\nabla x^i$. In the previous expressions, J_0 represents the gyro-average operator, which can be switched on or off. In case it is off, the gyro-average operator is simply reduced to the identity. In case it is on, it is computed as follows for a given quantity X: (1) for each particle, its local Larmor radius ρ_{local} is calculated, (2) a set of N_{avg} points $\{(r_i, \theta_i)\}_{1\leq i\leq N_{\mathrm{avg}}}$ is selected

on the circle with centre the particle and with radius ρ_{local} and (3) the gyro-averaged X is approximated as $J_0 \cdot X \approx \frac{1}{N_{\text{avg}}} \sum_i X(r_i, \theta_i)$. The gyro-average operator is applied to the electrostatic and magnetic potentials before computing the gradient. For the sake of simplification, it is assumed that gradient and gyro-average operators commute, i.e. $\nabla J_0 \cdot X = J_0 \cdot \nabla X$.

In TAPAS we use normalized quantities in such a way that distances are normalized to reference thermal Larmor radius

$$\rho_{\text{ref}} = \sqrt{\frac{T_{\text{ref}}}{m_{\text{ref}}}} \frac{m_{\text{ref}}}{e Z_{\text{ref}} B_{\text{ref}}} \tag{12}$$

and time is normalized to a reference cyclotron frequency

$$\omega_{c,\text{ref}} = \frac{e Z_{\text{ref}} B_{\text{ref}}}{m_{\text{ref}}} \tag{13}$$

and the velocity of the modelled species is normalized to its thermal velocity

$$v_{\text{th}} = \sqrt{\frac{T_{\text{ref}}}{m}} \tag{14}$$

The integration of the trajectories is done using a 4^{th} order explicit Runge-Kutta method (RK4) in toroidal coordinates. This method can raise the problem that the minor radius for particles close to the magnetic axis can take intermediate or final negative values, which is obviously mathematically forbidden. Therefore, for those particles the trajectories are integrated in cylindrical coordinates (R, Z, φ). Each particle is initialized with a given spatial position (r, θ, φ). The initialization in velocity space can be done using different coordinates: $\left(v_\parallel, \mu\right)$, (E, Λ), (E, P_φ) and (E, λ), where $\Lambda = \mu B_0 / E$, $\lambda = v_\parallel / v$ and P_φ is the toroidal canonical momentum. Once this initialization in velocity space is selected, the code performs a mapping onto $\left(v_\parallel, \mu\right)$. In the present work we use the initialization (E, λ). It is to be noted that the initialization can be done on a 5D grid of uniformly separated points or using a uniformly random loading. The former one is used in this work. In addition to the initial coordinates in 5D space, each particle is assigned a weight quantifying the number of physical particles represented by the computational particle. Such weight is calculated as

$$w_i = \int_{V_i} \mathrm{d}\tau^\star F \tag{15}$$

where $\mathrm{d}\tau^\star = J_v \mathrm{d}v_\parallel \mathrm{d}\mu \mathrm{d}r \mathrm{d}\theta \mathrm{d}\varphi$, V_i is the volume represented by the particle i and F is the distribution function. Particles can be initialized either uniformly or randomly in real space and velocity space.

2.2. Structure, parallelization and scaling of the code

The TAPAS software application, is a FORTRAN code parallelized over multi-GPU nodes. It uses a hybrid paradigm MPI-OpenACC. The Message Passing Interface (MPI) library describes a usual domain decomposition parallelism, over nodes, and between GPU within a node. OpenACC directives inside the FORTRAN source code describe the offload of the computation onto the GPU accelerator. This includes (1) the description

of data movement between the node memory and the GPU accelerator memory and (2) the description of fine grain parallelisms on loops over particles to take advantage of the multiple computational unit of GPU accelerator. TAPAS requires LAPACK library for the eigen-solver of Ampère's law to get the parallel magnetic potential. It also uses parallel HDF5 library and format for I/O. The steps of the simulation are as follows:

(i) Initialization of MPI and OpenACC.

(ii) Reading of input file.

(iii) A flag in the input file indicates whether the simulation must restart from a previous one or not. In case it is a restart, an HDF5 file containing the 5D coordinates of all the particles (called *restart file*) is read.

(iv) Computing of all the required metric quantities in case of a numerical/experimental equilibrium.

(v) Saving of the metric in an HDF5 file.

(vi) If required, computing of the parallel magnetic potential using the eigen-value solver.

(vii) If required, initialization of the quantities used by the gyro-average operator.

(viii) The initialization of particles is done, either by setting their coordinates to the ones read from the restart file or by initializing them to coordinates that are read from an input file (it can be on a uniform grid or randomly).

(ix) If it is not a restart, the initial 5D coordinates are stored in an HDF5 file.

(x) The temporal loop is started: the four steps of the RK4 integration is done for each particle. After each step of the RK4 scheme it is verified whether the minor radius takes negative values. In case it does, the trajectory is solved using cylindrical coordinates.

(xi) After each time step a verification is made to determine whether each particle has reached the wall or not. The code allows the possibility to continue the integration outside the tokamak. However, if this possibility is not activated the integration of the trajectory is stopped and the particle is labeled as lost.

(xii) Every n_{diag} time steps the diagnostics are applied to store 1D, 2D or 5D information.

(xiii) At the end of the temporal loop a restart file is produced.

All the simulations presented in this work have been run on the French Jean-Zay supercomputer, which is an HPE SGI 8600 computer composed of two partitions: a partition containing nodes with only CPU (CPU partition); and a partition containing accelerated nodes with four or eight GPU accelerators per node in addition to CPU (GPU or accelerated partitions). Nodes are linked by a fast low latency Omni-Path network with enhanced hypercube topology. The CPU partition is composed of 1528 nodes, with two Intel Cascade Lake 6248 processors, 40 cores each node, 192 GB of memory each node, and one Omni-Path network interface each node. The four-GPU partition (the one used in this work) is composed of 612 accelerated compute nodes with

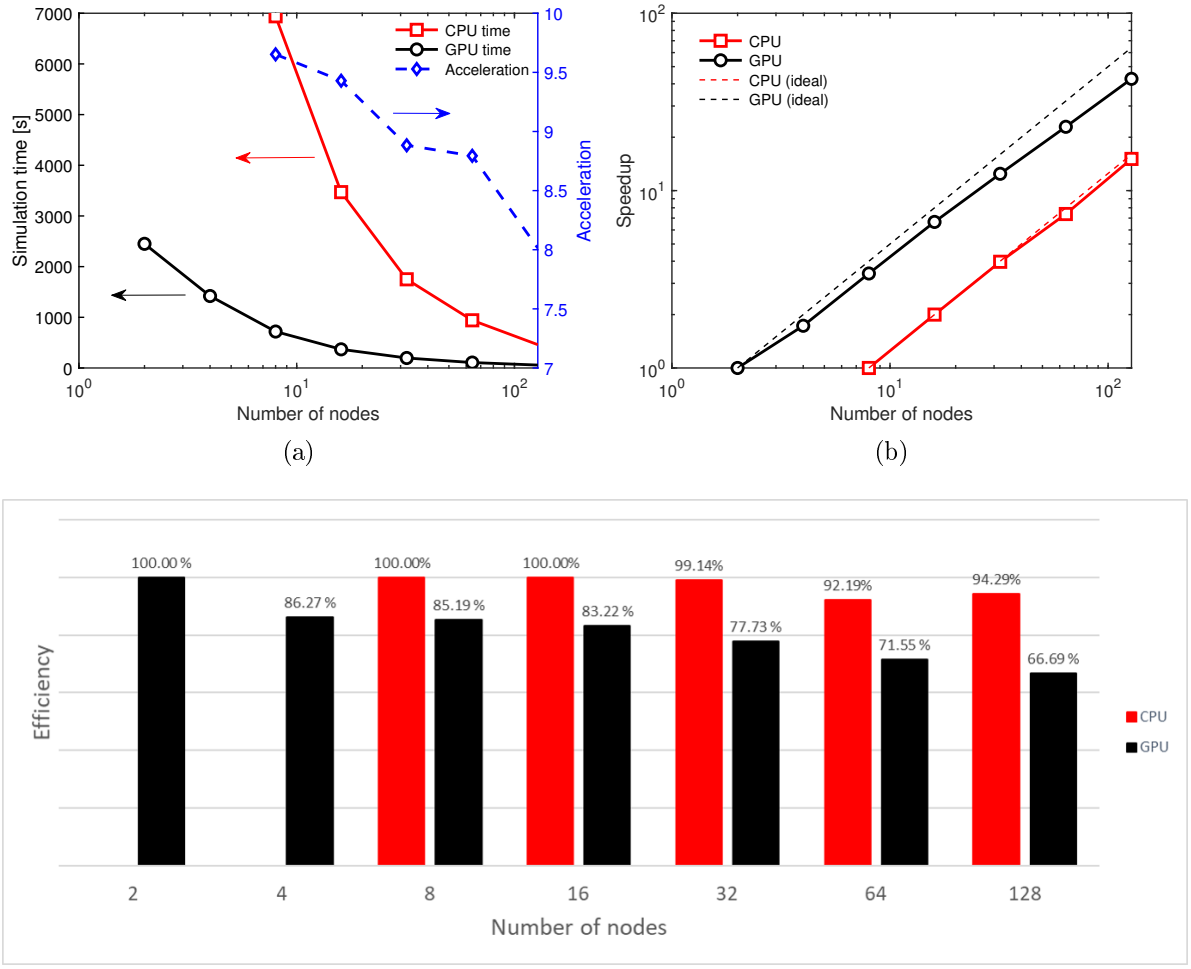

Figure 1: Simulation time (top left), speedup (top right) and efficiency (bottom) as a function of the number of nodes for CPU and GPU partitions on Jean-Zay supercomputer.

two Intel Cascade Lake 6248 processors, four NVIDIA Tesla V100 SXM2 GPUs (261 nodes with 16 GB and 351 nodes with 32 GB of memory), and four Omni-Path network interface each node. The code has been compiled using the FORTRAN compiler from the NVIDIA HPC software development kit. We have analysed the scaling of the code on Jean-Zay using a fixed-size test case with $\sim 1.3 \cdot 10^9$ alpha particles during 5000 time steps. The time of the simulation as a function of the number of nodes when running the fixed-size test case on the CPU and on the GPU partitions is given in figure 1a (left y-axis). The acceleration is defined as the ratio between the time on CPU nodes, with one MPI process (*aka* rank) per core, and the time on the same number of accelerated nodes, with four MPI processes per node (one rank per GPU). This acceleration is given on the right y-axis of the same figure. The acceleration factor starts at ~ 9.5 and

decreases with the number of nodes down to ~ 8. The speedup is provided in figure 1b for both partitions. It is defined as $\text{speedup}_N = t_N/t_{N0}$, where N is the number of nodes and $N0$ is the reference number of nodes (2 for the accelerated partition and 8 for the CPU partition). For each partition, the ideal scaling is represented by dashed lines. By *ideal* we mean that the simulation time is divided by n when multiplying the number of nodes by n. Finally, the efficiency is given in figure 1c for each partition as a function of the number of nodes and measured as the ratio between the speedup and the ideal speedup. It can be observed that, although the code tends to be closer to the ideal scaling on the CPU than on the GPU partition, its use on GPU allows a significant acceleration for a production case. In other words, for the same number of available computational nodes on CPU and GPU partitions, running the code on GPU provides an acceleration which compensates for the slightly reduced efficiency.

3. Simulation set-up

Although the magnetic field can be given numerically, in the present paper we use an axisymmetric equilibrium magnetic field of the form

$$\mathbf{B}_{\text{eq}} = B_0 R_0 \left(f\left(r\right) \nabla\varphi \times \nabla r + g\left(r\right) \nabla\varphi \right) \tag{16}$$

with

$$f\left(r\right) = \frac{r}{q\left(r\right) R_0} g\left(r\right) \tag{17}$$

and $q\left(r\right)$ the safety factor as a function of the minor radius. For the sake of simplicity here we impose concentric and circular flux surfaces, which implies $g\left(r\right) = 1$. Therefore, the toroidal magnetic field yields

$$B_\varphi = \frac{B_0 R_0}{R} \tag{18}$$

$$B_\theta = \frac{r}{q\left(r\right) R_0} B_\varphi \tag{19}$$

where $R = R_0 + r\cos\theta$. To investigate the effect of a tearing mode on the trajectories of energetic particles we impose a purely magnetic perturbation of the form $\mathbf{A} = A_\parallel\left(r,\theta,\varphi\right)\mathbf{b}$. The function $A_\parallel$ can be decomposed as $A_\parallel = A_{\parallel 0} A_\parallel\left(r\right)\cos\left(m\theta + n\varphi - \omega t\right)$, where (m, n, ω) are the poloidal and toroidal mode numbers and the island rotation frequency, respectively, and $A_{\parallel 0}$ is a constant that controls the amplitude of the perturbation and provides therefore the width of the magnetic island. The radial eigenfunction $A_\parallel\left(r\right)$ is calculated numerically using a shooting module, as done in [27], in a radial grid which can be as fine as required. The boundary conditions for $A_\parallel$ are $A_\parallel\left(r=0\right) = A_\parallel\left(r=a\right) = 0$ and we impose the continuity of the solution at r_{res}, i.e. $A_\parallel\left(r \to r_{\text{res}}^-\right) = A_\parallel\left(r \to r_{\text{res}}^+\right) \equiv A_\parallel\left(r = r_{\text{res}}\right)$, with r_{res} the position of the resonant surface where $q = m/n$. Therefore, the integration of the trajectories can be done using interpolated values of $A_\parallel\left(r\right)$ obtained from standard interpolation methods such as Lagrange polynomials. The toroidal and poloidal numbers and the frequency are fixed. Thus, the angular and temporal dependence can be

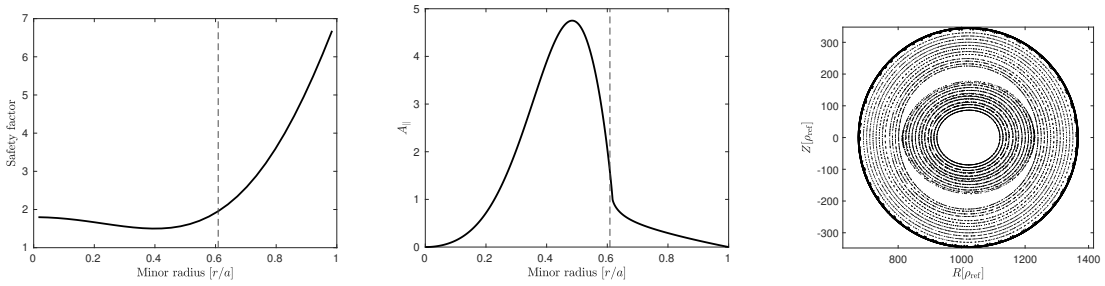

(a) (b) (c)

Figure 2: Radial profiles of safety factor (left) and magnetic potential computed using a linear eigen-solver (middle) together with the Poincaré map of the magnetic field lines in the presence of the magnetic perturbation $A_\parallel$ (right).

analytically evaluated. Because of the major role that alpha particles can play in future fusion devices and because of the presence of alpha particles in the current experimental campaign in the Joint European Torus (JET) device, in the following we show numerical results of a JET-like tokamak: we simulate alpha particles in a tokamak of the size of JET, but for the sake of numerical simplification we use concentric and circular flux surfaces. We use Deuterium as as normalizing species. Therefore $m_{\text{ref}} = 2m_p$, with m_p the proton mass, and $Z_{\text{ref}} = 1$. The reference temperature is $T_{\text{ref}} = 5$ keV and the reference magnetic field is $B_{\text{ref}} = 3.5$ T. The dimensions of the simulated tokamak in normalized units are $a = 345\rho_{\text{ref}}$, $R_0 = 1020\rho_{\text{ref}}$, with $\rho_{\text{ref}} = 1/345$ m. The mass and charge of the simulated alpha particles are $m = 2m_{\text{ref}}$ and $Z = 2Z_{\text{ref}}$, respectively. For fusion-born alpha particles, the energy is $E = 700E_{\text{th}}$, with $E_{\text{th}} = 5$ keV. The safety factor is slightly reversed, taking a minimum value of $q_{\text{min}} = 1.5$, an on-axis value $q_0 = 1.8$ and an edge-value $q_a = 7.0$. Such safety factor has been chosen to exhibit different rational surfaces $q = m/n$ and to be close to realistic reversed JET q-profiles [28]. This magnetic equilibrium is $(m = 2, n = 1)$ tearing unstable, i.e. $\Delta' > 0$, with Δ' the instability parameter calculated as

$$\Delta' = \frac{1}{A_\parallel\left(r = r_{\text{res}}\right)}\left(\lim_{r\to r_{\text{res}}^+}\frac{\mathrm{d}A_\parallel}{\mathrm{d}r} - \lim_{r\to r_{\text{res}}^-}\frac{\mathrm{d}A_\parallel}{\mathrm{d}r}\right) \tag{20}$$

The radial profiles of the safety factor and the magnetic potential are given in the left and middle panels of figure 2, respectively. The rational surface $q = m/n = 2$ is represented by a vertical dashed line. The total magnetic field $\mathbf{B} = \mathbf{B}_{\text{eq}} + \delta\mathbf{B}$, where $\delta\mathbf{B} = \nabla \times \left(A_\parallel \mathbf{b}\right)$, exhibits a magnetic island around the rational surface $q = 2$, as depicted in figure 2c.

In the absence of any drifts, charged particles should follow exactly the magnetic field lines. However, the finite Larmor radius induces a drift such that particle trajectories deviate from the magnetic surfaces. Such effect is more pronounced for EP (and even more significantly for alpha particles) than for thermal particles. A naive

reasoning would lead to the fact that the Poincaré map of the trajectories of alpha particles is simply the one illustrated in figure 2c but shifted to the right or to the left for co- or counter-passing particles, respectively. However, it was reported in [29] that the periodicity in the drift of EP trajectories can couple to the magnetic perturbation inducing a series of islands in the Poincaré map of the EP. Such effect is also observed in the simulations reported in the present work. The Poincaré map of deeply counter-passing alpha particle trajectories for different energies is illustrated in figure 3. Both left and right panels represent the same Poincaré maps, but using different coordinates. It is observed the formation of several islands that appear at different rational surfaces ($q = 3$, $q = 4$, $q = 5$, ...). Increasing the energy of alpha particles leads to the overlap of these islands resulting in chaos that can be responsible for the transport and losses of alpha particles, which is analysed in the next sections.

Fusion-born alpha particles can be modelled by the following distribution function

$$F_\alpha\left(r, E, \lambda\right) = n\left(r\right) \mathcal{U}_{[-1,1]}\left(\lambda\right) \delta\left(E - E_\alpha\right) \tag{21}$$

where $\lambda = v_\parallel / v$ is the cosine of the pitch angle, $n\left(r\right)$ is the radial profile of density, $\mathcal{U}_{[-1,1]}\left(\lambda\right)$ is a uniform distribution function between $\lambda = -1$ and $\lambda = 1$ and $\delta\left(E - E_\alpha\right)$ represents the Dirac distribution. In this work, we use a radial profile consistent with extrapolated DT scenarios in JET exhibiting peaked fusion-born alpha density profiles peaked in the inner region [28]. Figure 4a illustrates the initial radial profile of the density of alpha particles considered in this paper. The uniform distribution function $\mathcal{U}_{[-1,1]}\left(\lambda\right)$ does not result in a uniform distribution function in the motion invariant $\Lambda = \mu B_0 / E$. Such deviation is depicted in figure 4b, showing a PDF as a function of Λ, which exhibits a mean value $\langle\Lambda\rangle = \int \mathrm{d}\Lambda\, \mathcal{P}\left(\Lambda\right) \Lambda = 0.68$. Particles are tracked up to $\omega_{c,\mathrm{ref}} t = 10^7$, which represents ~ 60 ms. It is to be noted that this time is less than the expected thermalization time for alpha particles in JET, which is $\sim 300 - 500$ ms. Therefore, the simulations reported here are intended to characterize the transport and losses in a time-scale where collisions do not dominate the dynamics of alpha particles. The impact of the tearing mode is analysed by performing scans on the amplitude (and therefore on the magnetic island width) and on the rotation frequency. In order to minimize the computational cost of such scans, the alpha particles are represented by 10^7 markers initialized at $\varphi = 0$, i.e. we initialize a disk in (r, θ). Therefore, each particle represents physical particles in a domain $\left[r_{i-1/2}, r_{i+1/2}\right) \times \left[\theta_{i-1/2}, \theta_{i+1/2}\right) \times \left[0, 2\pi\right)$. Nonetheless, we have performed one single simulation where particles are initialized over several values of φ and the results do not change significantly.

4. Impact of the island width and frequency on the losses of fusion-born alpha particles

Figure 5 represents the final density radial profile (5a) and the number of confined particles as a function of Λ (5b). In this figure we show, as a reference, the initial profiles with thin solid black lines, whereas final profiles are given by thick lines. It is to be noted

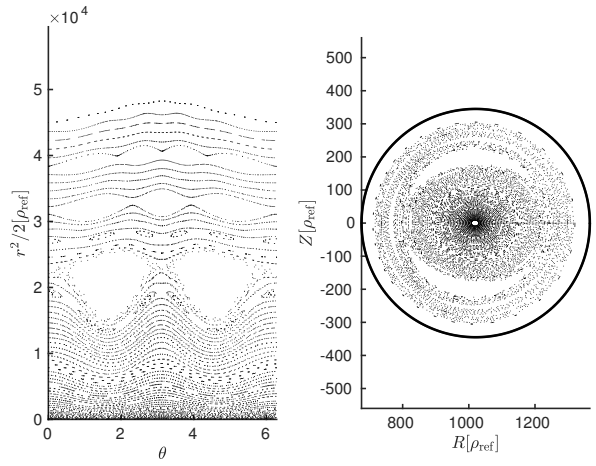

(a)

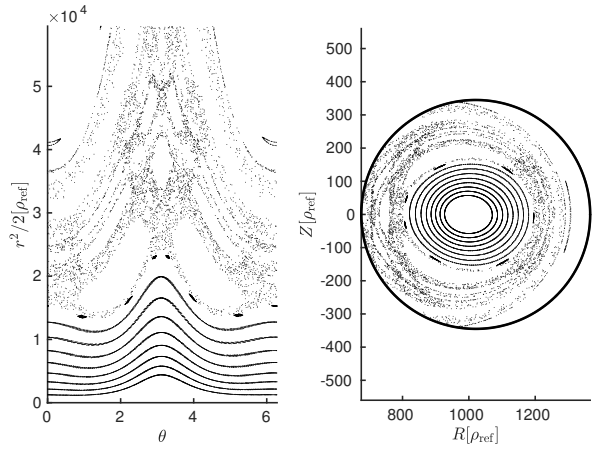

(b)

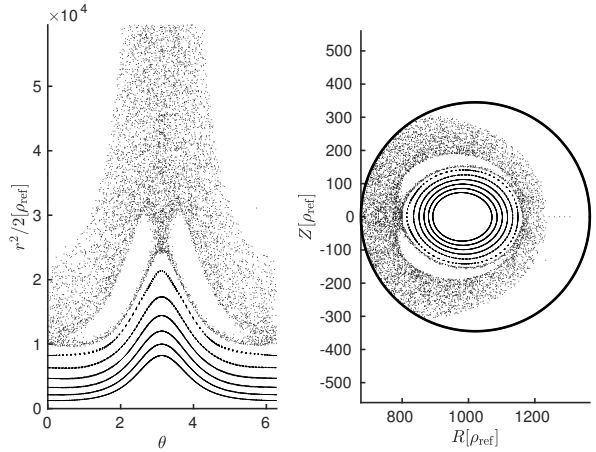

(c)

Figure 3: Poincaré map of deeply counter-passing alpha particle trajectories for three values of energy: $E = E_{\rm th}$ (top), $E = 200E_{\rm th}$ (middle) and $E = 700E_{\rm th}$ (bottom).

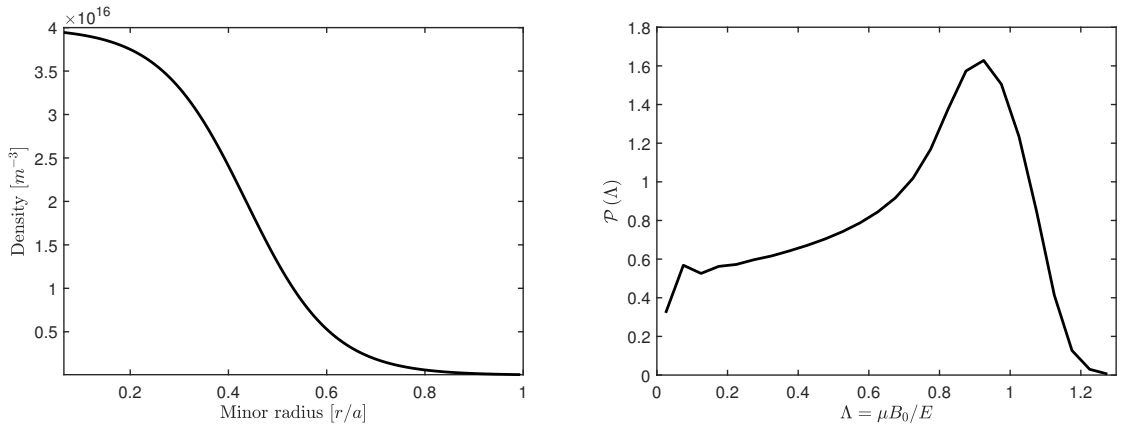

(a) (b)

Figure 4: Initial density profile (left) and probability density function in terms of Λ invariant (right).

that even in the absence of magnetic perturbation losses are observed, called prompt losses or firts orbit losses. Therefore, we must compare the final profiles with (solid red line) and without (dashed blue line) tearing mode. The final profiles in the presence of tearing mode are obtained with a static ($\omega = 0$) magnetic perturbation characterized by an amplitude $A_{\parallel 0} = 0.05$, which represents an island half-width $w_{\text{isl}} \approx 7 \cdot 10^{-2}$ m. It is observed that prompt losses lead to significant modifications of the initial profiles. The impact of the tearing mode results in additional losses mainly in the radial region $0.2 < r/a < 0.8$. In addition, figure 5b shows that the tearing mode impacts strongly the confinement of alpha particles with $\Lambda < 1$, although the mean value $\langle \Lambda \rangle = 0.63$ remains close to the initial one.

More in-depth analysis can reveal the confinement of particles depending on their trajectories. Figure 6a represents the number of physical particles that are confined in the tokamak as a function of the pitch angle λ. The thin solid black line indicates the initial number of particles, which does not depend on λ since particles are initialized with a uniform distribution function. The dashed blue line represents the number of confined particles in the absence of the magnetic perturbation, whereas the solid red line gives the number of confined particles in the presence of a tearing mode of amplitude $A_{\parallel 0} = 0.05$, i.e. $w_{\text{isl}} = 7 \cdot 10^{-2}$ m. It is to be noted that although the value of λ does not necessarily determine the class of trajectory it is useful to establish general behaviour for deeply passing ($|\lambda| = 1$) or deeply trapped ($\lambda \approx 0$). Based on this fact, this figure deserves two comments. First, it is observed that co-passing particles are not significantly affected by prompt losses. Second, the tearing mode seems to affect mainly (co- and counter-) passing particles and only slightly trapped particles. Further information can be gained by classifying exactly each simulated particle into one of the three possible groups of trajectory: co-passing ($v_{\parallel} > 0$), counter-passing ($v_{\parallel} < 0$) or

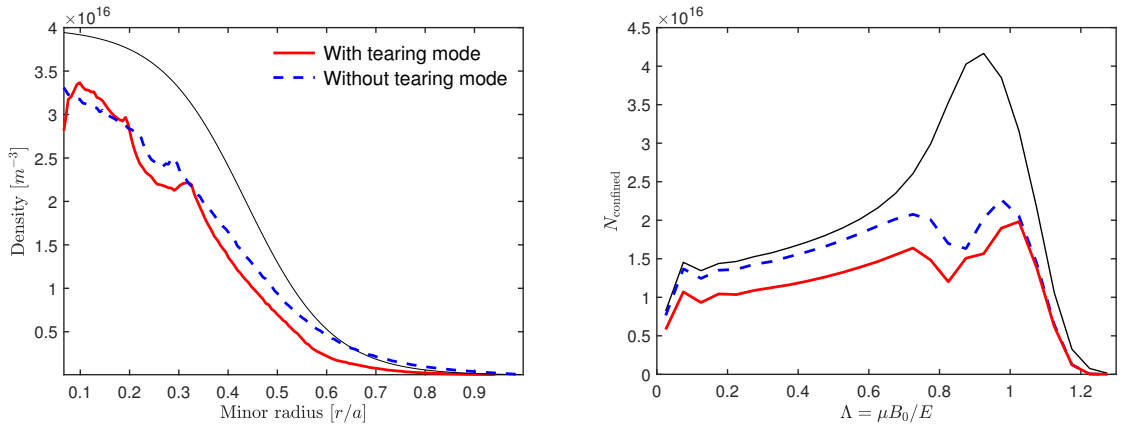

(a) (b)

Figure 5: Final density profile (left) and number of confined particles in terms of Λ invariant (right).

trapped ($v_\parallel$ changes its sign). It is to be noted that this classification is done based on the unperturbed parallel motion. This means that the so-called stagnation orbits are naturally included in the ensemble of co-passing particles. Indeed, stagnation orbits correspond to the orbits of particles that circulate toroidally while keeping their poloidal angle almost unchanged. We compute the effective fraction of lost particles for each group of trajectories, $f_{\text{lost}} = N_{\text{lost}}/N_{\text{total}}$, where

$$N_{\text{lost}} = N_{\text{lost}}^{\text{with}} - N_{\text{lost}}^{\text{w/o}} \tag{22}$$

$$N_{\text{total}} = N_{\text{init}} - N_{\text{lost}}^{\text{w/o}} \tag{23}$$

with $N_{\text{lost}}^{\text{with}}$ (resp. $N_{\text{lost}}^{\text{w/o}}$) representing the number of particles lost in the presence (resp. in the absence) of a tearing mode and N_{init} represents the total number of initialized particles. The dependence of f_{lost} on the width of a static ($\omega = 0$) magnetic island is given in figure 6b for co-passing (squares), counter-passing (diamonds) and trapped (stars) particles. Open circles indicate f_{lost} for all classes of particles. It is observed that, as already anticipated in figure 6a, mainly passing particles are affected by the magnetic perturbation and trapped particles are less affected. Also, the fraction of lost particles increases non-linearly with the width of the magnetic island.

The previous results have been obtained with a static magnetic island, i.e. $\omega = 0$. It is to be noted that tearing modes are characterized by a finite rotation frequency, which can evolve depending on the regime where the island is generated. Indeed, in the absence of turbulence and in linear collisionless regime the magnetic island rotates in the electron diamagnetic frequency [30]. However, when turbulence is present the magnetic island can interact nonlinearly with the turbulent modes and the rotation frequency can be reversed, i.e. the magnetic island rotates at the ion diamagnetic

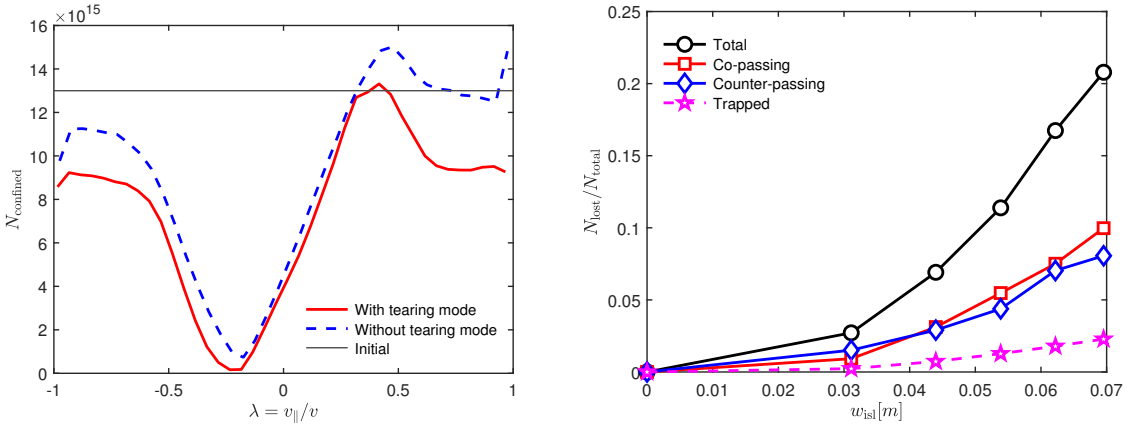

(a) (b)

Figure 6: Left: number of confined particles at the beginning of the simulation (horizontal line) and at the end of the simulation in the absence (blue dashed line) and in the presence (solid red line) of tearing mode. Right: effective fraction of lost particles f_{lost} as defined in the text for co-passing (squares), counter-passing (diamonds) and trapped (stars) particles, together with the sum of the contributions of each class of trajectory (circles).

direction [31]. Therefore, it is essential to perform a scan on the frequency of the magnetic perturbation in order to assess the impact of the tearing mode on fusion-born alpha particles in different regimes. The scan over the island width has been performed also with finite island rotation. The result is shown in figure 7 for positive (7a) and negative (7b) frequency. The value $\omega = 10^{-3}\omega_{\text{c,ref}}$ corresponds to $f_{\text{isl}} \approx 24$ kHz, which is an upper bound for the rotation frequency of magnetic islands. Our simulations indicate that positive rotation frequencies tend to deconfine co-passing particles and confine counter-passing particles with respect to the situation of static magnetic island. On the other hand, negative rotation frequencies tend to reverse this phenomenon. The better confinement of co-passing or counter-passing particles implies an asymmetry in the alpha distribution function which can potentially generate a net momentum.

To understand why the rotation frequency can impact the confinement of alpha particles we must study the fundamental mechanism of wave-particle interaction. The unperturbed motion of particles in a tokamak can be described by the set of action-angle variables $(\boldsymbol{\alpha}, \mathbf{J})$, with $\boldsymbol{\alpha} = (\alpha_1, \alpha_2, \alpha_3)$ and $\mathbf{J} = (J_1, J_2, J_3)$. The first angle α_1 is actually equivalent to the gyrophase, i.e. $\alpha_1 \equiv \varphi_c$, and the associated invariant J_1 is proportional to the adiabatic moment μ. The second angle is related to the motion of particles in the poloidal plane and the third angle is related to the motion of particles in the toroidal direction. In the presence of a mode $\exp(n_2\alpha_2 + n_3\alpha_3 - \omega t)$, particles can resonate if their velocities are close to the phase velocity of the wave, which translates

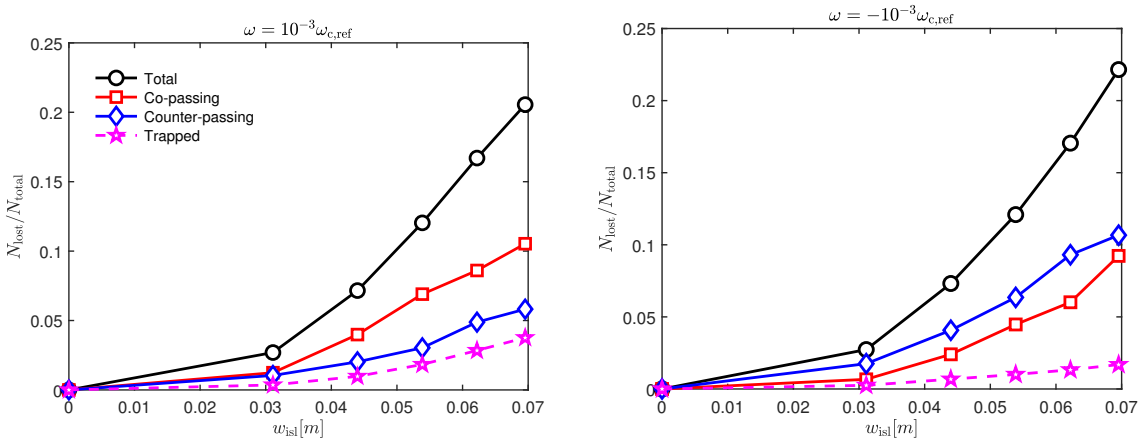

(a) (b)

Figure 7: Same as figure 6b, but with rotating magnetic islands: $\omega = 10^{-3}\omega_{c,ref}$ (left) and $\omega = -10^{-3}\omega_{c,ref}$ (right), corresponding to a rotation frequency $f_{isl} \approx 24$ kHz.

into [32]

$$\omega - n_2\Omega_2 - n_3\Omega_3 \approx 0 \tag{24}$$

where $\Omega_2 = \dot{\alpha}_2$ and $\Omega_3 = \dot{\alpha}_3$. This resonance condition has been studied also in previous works of transport and losses of EP. For instance, in the presence of Alfvén eigenmodes (eq. (1) of Ref. [33]) and in the presence of static ($\omega = 0$) resonant magnetic perturbations [34]. Note that in this work the tearing mode is characterized by one single helicity (m, n), but the significant drift of fusion born alpha particles results in the formation of several n_2 harmonics, i.e. $n_2 = 1, 2, 3, \ldots$. On the other hand, the mode number n_3 associated with the toroidal motion satisfies $n_3 = n$. Computing the characteristic frequencies Ω_2 and Ω_3 allows us to determine the resonances that can potentially exist. The calculation of the frequencies is done as follows. We compute the Fourier transform of $r - \langle r \rangle_t$, where $\langle \cdot \rangle_t$ represents an average over the trajectory. The frequency Ω_2 corresponds then to the frequency of the maximum Fourier mode in absolute value. As for Ω_3, it is calculated as $\Omega_3 = \langle \dot{\varphi} \rangle_t$. In order to have a 2D representation, we analyse only the resonance condition 24 for alpha particles initialized at $\theta = 0$. Such representation is given as a function of (r, λ) in figure 8 for the three analysed frequencies: $\omega = -10^{-3}\omega_{c,ref}$ (top row), $\omega = 0$ (middle row) and $\omega = 10^{-3}\omega_{c,ref}$ (bottom row). The resonances are plotted with different coloured lines: $n_2 = 1$ (dashed grey), $n_2 = 2$ (black), $n_2 = 3$ (red), $n_2 = 4$ (magenta) and $n_2 = 5$ (yellow). These labels are indicated only in the upper-left panel for the sake of clarity. Together with the resonances, in the left colum the green region corresponds to co- and counter-passing particles, the blue region represents trapped particles and the white area indicates the region of prompt losses. In the panels of the right column we provide also the probability to exit the tokamak ($\mathcal{P}_{exit}$) for a particle born with given (r, λ).

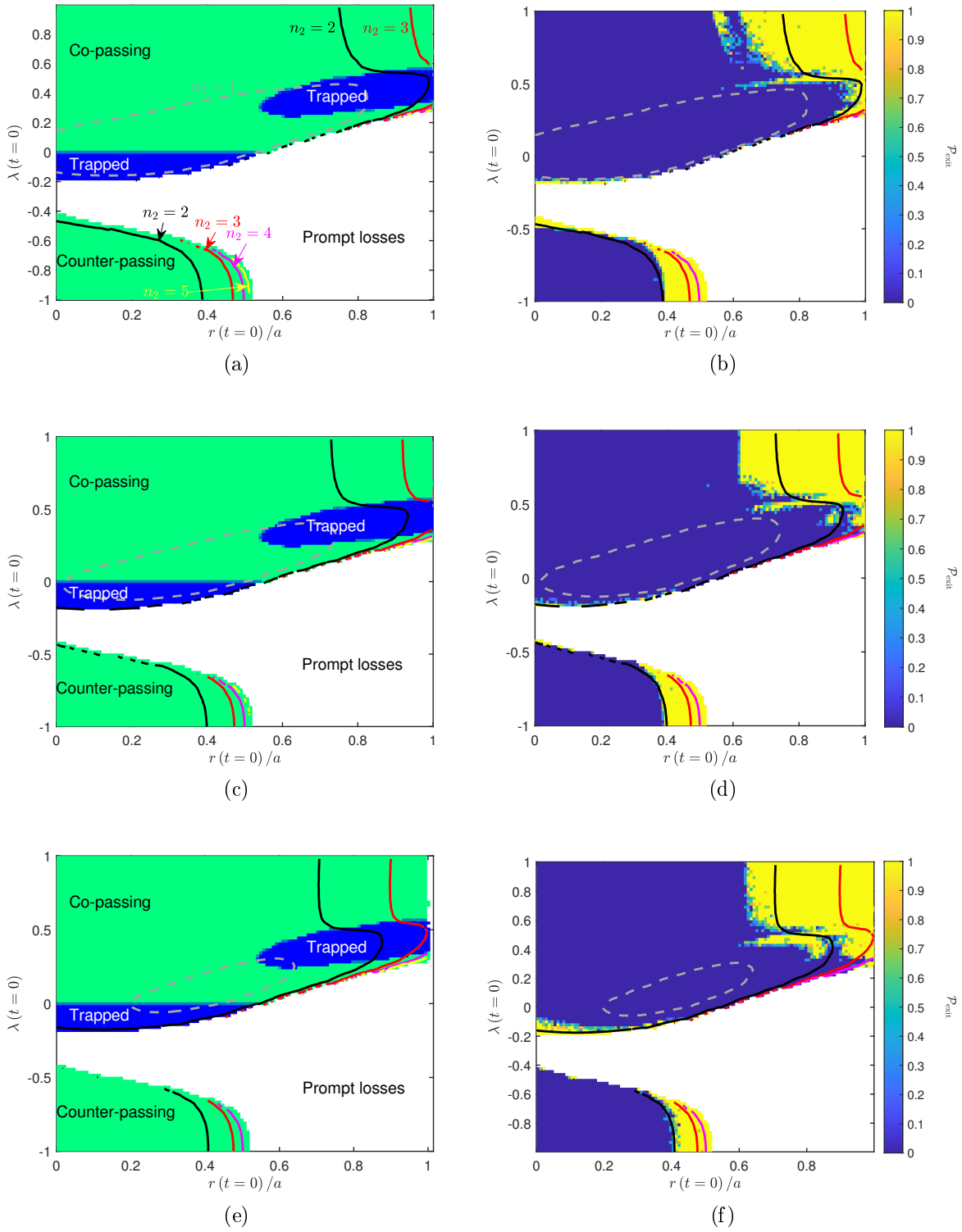

Figure 8: Contours of the resonance condition 24 for different values of n_2 as a function of (r, λ) for $\omega = -10^{-3}\omega_{c,\mathrm{ref}}$ (top row), $\omega = 0$ (middle row) and $\omega = 10^{-3}\omega_{c,\mathrm{ref}}$ (bottom row). In the left column the resonances are plotted together with the classes of trajectories and the region of promp losses. In the right column the mean exit probability is also represented.

It is to be noted that similar diagrams were given in figure 25 of Ref. [33], where also the so-called stagnation orbits were represented. Such orbits are naturally embedded in the co-passing region of the present work, as explained earlier, and therefore they are not indicated in figure 8. It is observed that the loss region, characterized by a high $\mathcal{P}_{\text{exit}}$ appears where the resonances occur, which is consistent with the overlap of the different resonances leading to the formation of a chaotic region, as already observed with other modelling studies of EP losses in AUG and DIII-D [33]. It is to be noted that analyses of RMP-induced transport and losses of NBI-generated EP in AUG also demonstrated the role of linear resonances for weak perturbations and nonlinear resonances for strong perturbations [34]. However, no clear signature of nonlinear resonances has been observed in our work. The resonances are mainly present in the co- and counter-passing regions, which explains why in figures 6 and 7 the fraction of lost trapped particles is less than that of co- and counter-passing particles. Moreover, it is observed that a finite rotation frequency modifies the resonances in the plane (r, λ). In particular, negative rotation frequencies (in the electron diamagnetic direction) pushes the resonances to the inner part of the counter-passing region (decreasing r/a and λ) and to the outer part of the co-passing region (closer to the white or prompt losses region). Thus, counter-passing particles are more affected by the pertubation rotating in the electron diamagnetic direction than co-passing particles, resulting in increased f_{lost} for counter-passing particles. On the other hand, a positive rotation frequency (in the ion diamagnetic direction) leads to the opposite result. In addition, it can be observed that the resonances are pushed further into the trapped region located at $0.25 \leq \lambda \leq 0.5$. This explains why positive rotation frequencies can result in increased fraction of trapped particles.

5. Island-driven non-diffusive transport of fusion-born alpha particles

In order to characterize the transport of fusion-born alpha particles it is essential to perform statistical analysis of the exit process. This is because the time particles take to exit the tokamak and how the tail of the probability of this time scales determine the nature of the transport, as explained in [4]. For this purpose, we define the exit time, t_{exit}, as the time particles take to reach the wall from the moment they are initialized. Taking into account that for each position (r, θ) particles are initialized with all pitch angles $-1 \leq \lambda \leq 1$, and in order to simplify the visualization we compute two quantities: the mean exit probability $\langle \mathcal{P}_{\text{exit}} \rangle (r, \theta)$ and the mean exit time $\langle t_{\text{exit}} \rangle (r, \theta)$. The mean exit probability is defined as the probability that a particle initialized at (r, θ) is lost at $t \leq t_{\max}$. The mean exit time is defined as the most probable time that a particle initialized at (r, θ) takes to be reach the radial position $r = a$. Note that the mean probability and the mean exit time are calculated up to $\omega_{\text{c,ref}} t_{\max} = 10^7$. Such quantities can also be decomposed into co-passing, counter-passing and trapped particles and are plotted in figure 9. The top panels represent the mean exit probabilities for counter-passing (9a), trapped (9b) and co-passing (9c) particles. The bottom panels represent

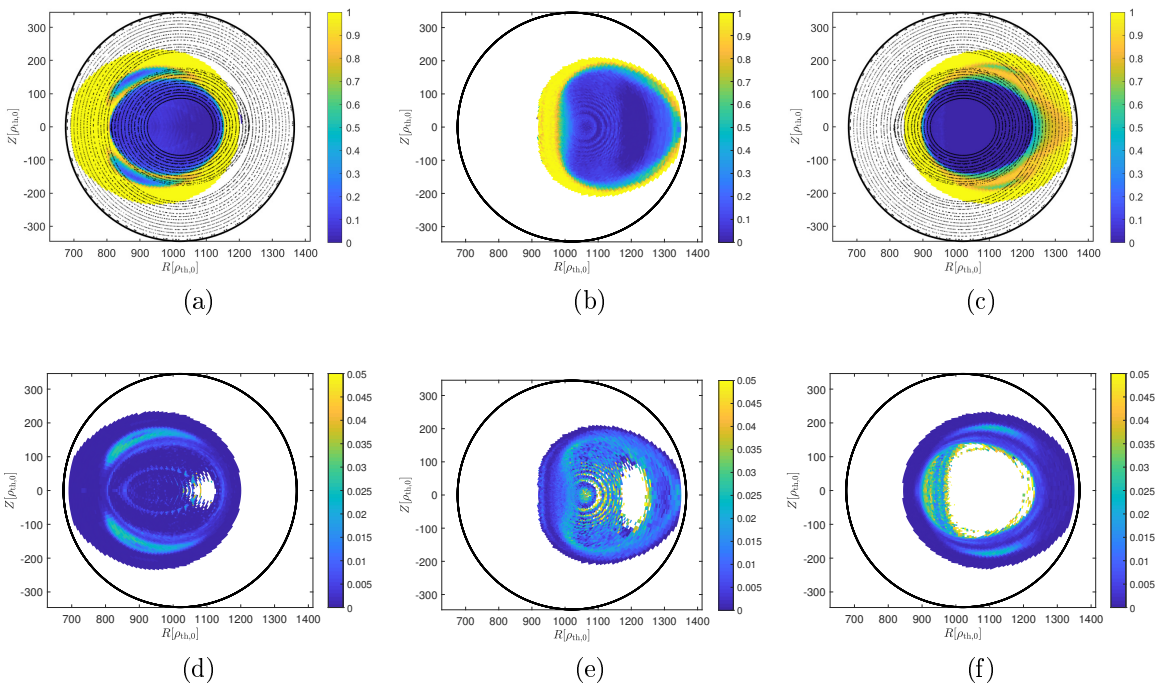

Figure 9: Mean exit probability (top row) and mean exit time expressed in seconds (bottom row) for counter-passing (left column), trapped (middle column) and co-passing (right column) particles. Together with the mean exit probabilities for counter- and co-passing particles overlaid is the Poincaré map of the magnetic field lines.

the mean exit time expressed in seconds for the same groups of particles. For co- and counter-passing particles a clear up-down symmetric structure is observed. Such structure is reminiscent of the (m, n) magnetic island, as can be evidenced from the Poincaré map of the magnetic field that is overlaid. Due to the magnetic drift of alpha particles, the mean exit probability is shifted with respect to the Poincaré map of the magnetic field lines.

Such analysis indicates the existence of exit events occurring at long times with low probability. These events are therefore representative of the tail of the probability density function (PDF) of the exit time. As explained earlier, the statistics of these events, also known as *rare events*, is of prime importance for the characterization of the nature of the transport that fusion-born alpha particles can experience. For this purpose we compute the PDF of exit times $\mathcal{P}_{\text{exit}}$ taking into account all classes of particles (co-passing, counter-passing and trapped) lost only in the presence of the tearing mode. In that respect, it is useful to remind that diffusive transport is characterized by a PDF exhibiting an exponential scaling ($\mathcal{P}_{\text{exit}} \sim \mathrm{e}^{-\mu_e t}$) [35]. A simple exercise reported in [4] based on Monte-Carlo simulations of particles initialized in a disk showed such scaling. The PDF of the exit time computed from our simulations is plotted in log-log scale in figure 10a for different widths of a static ($\omega = 0$) magnetic island. It is observed

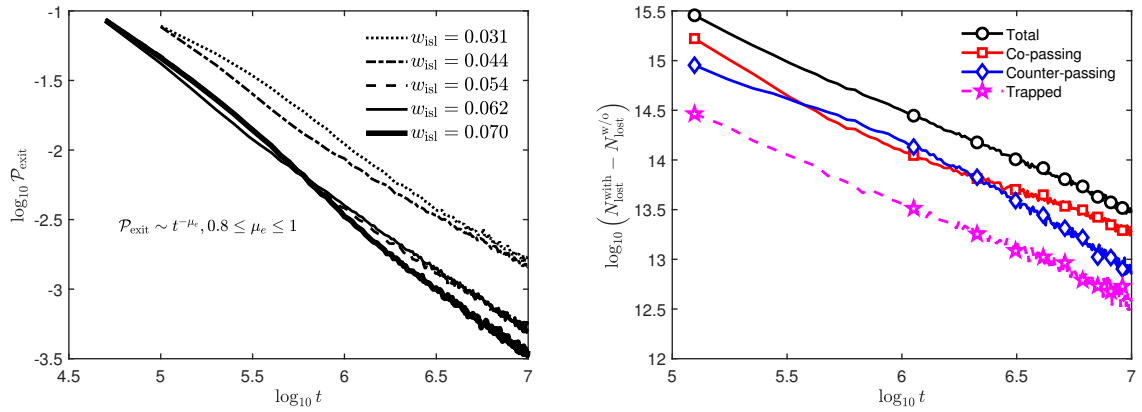

(a) (b)

Figure 10: PDF of the exit time for all classes of particles lost only in the presence of tearing mode as a function of the magnetic island width for $\omega = 0$.

that all of them the PDF exhibits algebraic scaling $\mathcal{P}_{\rm exit} \sim t^{-\mu_e}$. A fit of the tail of the PDF shows that $0.8 \leq \mu_e \leq 1$. Similar scaling has been observed for rotating magnetic islands (not shown here for the sake of simplicity). The fact that $\mu_e < 1$ implies that the mean exit time and all the higher order moments do not exist. Such scaling is characteristic of anomalous transport and was observed for the case of energetic particles transported in the presence of an oscillating radial electric field characterizing energetic geodesic acoustic modes [4]. The contribution of each class of particle to the algebraic scaling reveals that the tail of the PDF of the exit time is dominated by co- and counter-passing particles. However, the algebraic scaling observed in figure 10a is not necessarily present in all classes of trajectories. This observation is summarized in figure 10b, where the number of particles which are lost with a give exit time is represented in log-log scale for $w_{\rm isl} = 0.062$ for each class of trajectory. Whereas trapped particles exhibit a clear linear scaling, co- and counter-passing particles do not. It is to be noted that this classification into co-passing, counter-passing and trapped particles is based on the unperturbed motion.

6. Summary and future directions

In this work we have studied the transport and losses of (mono-energetic) fusion-born alpha particles in a JET-like tokamak. For this purpose, we have used the recently developed Toroidal Accelerated PArticle Simulator (TAPAS), which includes 3D electromagnetic perturbations, arbitrary magnetic equilibrium and is accelerated on GPU architecture. Here, we have used TAPAS to integrate the trajectories of guiding-centres under the simplification of concentric circular flux surfaces in the presence of an imposed single helicity magnetic perturbation representing a tearing mode. Such

perturbation leads to the formation of a magnetic island and we have studied both the impact of the island width and rotation frequency. It has been confirmed that the large magnetic drift of alpha particles leads to the formation of higher poloidal harmonics in phase space, which can eventually overlap and result in chaotic regions. These regions can increase the radial transport of fusion-born alpha particles and produce significant losses. We have indeed found that the region in phase-space where the losses occur are populated by the different resonances which can overlap. An extrapolated density profile for alpha particles in a DT plasma of the JET tokamak has been used to quantify and characterize the transport and losses of alpha particles in terms of the island width and rotation frequency. Our results show that the rotation frequency can modify the fraction of lost particles depending on the class of trajectory. Magnetic islands rotating at the electron (resp. ion) diamagnetic frequency tend to de-confine more counter-passing particles (resp. co-passing and trapped particles). This behaviour has been explained based on the modification of the linear resonances in phase space when the rotation frequency is modified. For negative frequencies, the resonances are more present in the region of counter-passing particles. On the other hand, for positive frequencies the resonances tend to be more present in the region of co-passing and trapped particles. Finally, the exit time, measured as the time a particle takes to reach the tokamak wall, has been computed. We have shown that the probability density function of the exit time exhibits algebraic decay of the form $\mathcal{P}_{\text{exit}} \sim t^{-\mu_e}$, with $\mu_e < 1$. This implies that the transport of fusion-born alpha particles due to tearing modes is not diffusive. It is to be noted that the work reported here needs to be extended to take into account the continuous generation of alpha particles for a realistic prediction of the modification of the radial profiles in the presence of a tearing mode. Also, including collisions and gyro-average effects will be done in the near future. Moreover, the parallelization and GPU acceleration of TAPAS is independent of the orbit model. Although in this work the guiding-centre model is used, it is to be noted that the structure of the code does not depend on the model. In particular, in the future full-orbit simulations will be presented and compared to the guiding-centre simulations.

Acknowledgments

This work has been carried out within the framework of the EUROfusion Consortium and has received funding from the Euratom research and training programme 2014-2018 and 2019-2020 under grant agreement No 633053. The views and opinions expressed herein do not necessarily reflect those of the European Commission. This work was granted access to the HPC resources of IDRIS under the allocation 2021-A0100512455 made by GENCI. D.d.-C.-N. was sponsored by the Oak Ridge National Laboratory, managed by UT-Battelle, LLC, for the US Department of Energy under Contract no. DE-AC05-00OR22725. Finally, TAPAS development, optimization and deployment on GPU accelerator were done within the framework of an advanced support program funded by IDRIS and GENCI.

References

[1] WW Heidbrink and GJ Sadler. The behaviour of fast ions in tokamak experiments. *Nuclear Fusion*, 34(4):535, 1994.

[2] SE Sharapov, B Alper, D Borba, L-G Eriksson, A Fasoli, RD Gill, A Gondhalekar, C Gormezano, RF Heeter, GTA Huysmans, et al. Energetic particle physics in jet. *Nuclear Fusion*, 40(7):1363, 2000.

[3] David Zarzoso, D del Castillo-Negrete, DF Escande, Y Sarazin, X Garbet, V Grandgirard, C Passeron, G Latu, and S Benkadda. Particle transport due to energetic-particle-driven geodesic acoustic modes. *Nuclear Fusion*, 58(10):106030, 2018.

[4] David Zarzoso and Diego del Castillo-Negrete. Anomalous losses of energetic particles in the presence of an oscillating radial electric field in fusion plasmas. *Journal of Plasma Physics*, 86(2), 2020.

[5] William A Newcomb. *Annals of Physics*, 10(2):232–267, 1960.

[6] Harold P Furth, John Killeen, and Marshall N Rosenbluth. *Physics of Fluids (1958-1988)*, 6(4):459–484, 1963.

[7] HP Furth, PH Rutherford, and H Selberg. *Physics of Fluids (1958-1988)*, 16(7):1054–1063, 1973.

[8] HE Mynick. Stochastic transport of mev ions by low-n magnetic perturbations. *Physics of Fluids B: Plasma Physics*, 5(7):2460–2467, 1993.

[9] SJ Zweben, DS Darrow, ED Fredrickson, G Taylor, S Von Goeler, and RB White. Mhd induced alpha particle loss in tftr. *Nuclear Fusion*, 39(9):1097, 1999.

[10] EM Carolipio, WW Heidbrink, CB Forest, and RB White. Simulations of beam ion transport during tearing modes in the diii-d tokamak. *Nuclear fusion*, 42(7):853, 2002.

[11] M García-Muñoz, P Martin, H-U Fahrbach, M Gobbin, S Günter, M Maraschek, L Marrelli, H Zohm, et al. Ntm induced fast ion losses in asdex upgrade. *Nuclear fusion*, 47(7):L10, 2007.

[12] William W Heidbrink, Laszlo Bardoczi, Cami S Collins, Gerrit J Kramer, Robert J La Haye, DJ Lin, Christopher M Muscatello, Mario Podesta, Luke Stagner, Michael A Van Zeeland, et al. The phase-space dependence of fast-ion interaction with tearing modes. *Nuclear Fusion*, 58(8):082027, 2018.

[13] Limin Yu, Erbing Xue, Debing Zhang, Shuyu Zheng, Xianmei Zhang, Juan Huang, Erzhong Li, Zheng-Mao Sheng, and Jing Fu. Simulation of the loss of passing fast ions induced by magnetic islands in east tokamak plasmas. *AIP Advances*, 11(2):025020, 2021.

[14] Dieter Biskamp. *Physics of Fluids (1958-1988)*, 29(5):1520–1531, 1986.

[15] FL Waelbroeck. *Nuclear Fusion*, 49(10):104025, 2009.

[16] RB t White and MS Chance. Hamiltonian guiding center drift orbit calculation for plasmas of arbitrary cross section. *The Physics of fluids*, 27(10):2455–2467, 1984.

[17] K Tobita, K Tani, Y Neyatani, AAE Van Blokland, S Miura, T Fujita, H Takeuchi, T Nishitani, M Matsuoka, and S Takechi. Ripple-trapped loss of neutral-beam-injected fast ions in jt-60u. *Physical review letters*, 69(21):3060, 1992.

[18] RJ Akers, LC Appel, PG Carolan, NJ Conway, GF Counsell, M Cox, SJ Gee, MP Gryaznevich, R Martin, AW Morris, et al. Neutral beam heating in the start spherical tokamak. *Nuclear fusion*, 42(2):122, 2002.

[19] GJ Kramer, RV Budny, A Bortolon, ED Fredrickson, GY Fu, WW Heidbrink, R Nazikian, E Valeo, and MA Van Zeeland. *Plasma Physics and Controlled Fusion*, 55(2):025013, 2013.

[20] Eero Hirvijoki, Otto Asunta, Tuomas Koskela, Taina Kurki-Suonio, Juho Miettunen, Seppo Sipilä, Antti Snicker, and Simppa Äkäslompolo. Ascot: Solving the kinetic equation of minority particle species in tokamak plasmas. *Computer Physics Communications*, 185(4):1310–1321, 2014.

[21] L Carbajal, D del Castillo-Negrete, D Spong, S Seal, and L Baylor. Space dependent, full orbit effects on runaway electron dynamics in tokamak plasmas. *Physics of Plasmas*, 24(4):042512, 2017.

[22] Mario Podesta, Marina Gorelenkova, and RB White. A reduced fast ion transport model for the

tokamak transport code transp. *Plasma Physics and Controlled Fusion*, 56(5):055003, 2014.

[23] L Bardóczi, M Podestà, WW Heidbrink, and MA Van Zeeland. Quantitative modeling of neoclassical tearing mode driven fast ion transport in integrated transp simulations. *Plasma Physics and Controlled Fusion*, 61(5):055012, 2019.

[24] J Yang, M Podestà, and ED Fredrickson. Synergy of coupled kink and tearing modes in fast ion transport. *Plasma Physics and Controlled Fusion*, 63(4):045003, 2021.

[25] SH Ward, Rob Akers, AS Jacobsen, P Ollus, SD Pinches, E Tholerus, RGL Vann, and MA Van Zeeland. Verification and validation of the high-performance lorentz-orbit code for use in stellarators and tokamaks (locust). *Nuclear Fusion*, 61(8):086029, 2021.

[26] Virginie Grandgirard, Jérémie Abiteboul, Julien Bigot, Thomas Cartier-Michaud, Nicolas Crouseilles, Guilhem Dif-Pradalier, Ch Ehrlacher, Damien Esteve, Xavier Garbet, Ph Ghendrih, et al. A 5d gyrokinetic full-f global semi-lagrangian code for flux-driven ion turbulence simulations. *Computer Physics Communications*, 207:35–68, 2016.

[27] D Zarzoso, S Nasr, X Garbet, A.I. Smolyakov, and S Benkadda. Gyro-kinetic theory and global simulations of the collisionless tearing instability: the impact of trapped particles through the magnetic field curvature. *Physics of Plasmas*, 2019.

[28] RJ Dumont, J Mailloux, V Aslanyan, M Baruzzo, CD Challis, I Coffey, A Czarnecka, E Delabie, Jacob Eriksson, J Faustin, et al. Scenario development for the observation of alpha-driven instabilities in jet dt plasmas. *Nuclear Fusion*, 58(8):082005, 2018.

[29] Harry E Mynick. Transport of energetic ions by low-n magnetic perturbations. *Physics of Fluids B: Plasma Physics*, 5(5):1471–1481, 1993.

[30] JF Drake, TM Antonsen Jr, AB Hassam, and NT Gladd. Stabilization of the tearing mode in high-temperature plasma. *The Physics of fluids*, 26(9):2509–2528, 1983.

[31] William A Hornsby, Pierluigi Migliano, Rico Buchholz, Stefan Grosshauser, Arne Weikl, David Zarzoso, Francis J Casson, Emanuele Poli, and Artur G Peeters. The non-linear evolution of the tearing mode in electromagnetic turbulence using gyrokinetic simulations. *Plasma Physics and Controlled Fusion*, 58(1):014028, 2015.

[32] D Edery, X Garbet, J P Roubin, and A Samain. Variational formalism for kinetic-mhd instabilities in tokamaks. *Plasma Physics and Controlled Fusion*, 34(6):1089, 1992.

[33] MA Van Zeeland, WW Heidbrink, RK Fisher, Manuel García Muñoz, GJ Kramer, DC Pace, RB White, S Aekaeslompolo, ME Austin, JE Boom, et al. Measurements and modeling of alfvén eigenmode induced fast ion transport and loss in diii-d and asdex upgrade. *Physics of Plasmas*, 18(5):056114, 2011.

[34] L Sanchis, M Garcia-Munoz, A Snicker, DA Ryan, David Zarzoso, Liu Chen, J Galdon-Quiroga, M Nocente, JF Rivero-Rodriguez, M Rodriguez-Ramos, et al. Characterisation of the fast-ion edge resonant transport layer induced by 3d perturbative fields in the asdex upgrade tokamak through full orbit simulations. *Plasma Physics and Controlled Fusion*, 61(1):014038, 2018.

[35] C. W. Gardiner. *Handbook of stochastic methods*. Springer Verlag, 2004.